Synthesis, electron diffraction, XRD and DSC study of the new elpasolite-related oxyfluoride, $Tl_3MoO_3F_3$

F.J. Brink,* L. Norén, and R.L. Withers

Research School of Chemistry, Australian National University, Canberra ACT 0200, Australia

Received 22 November 2002; received in revised form 10 March 2003; accepted 15 March 2003

Abstract

$Tl_3MoO_3F_3$, a previously unreported member of the $A_2BM^{VI}O_3F_3$ family of elpasolite-related oxyfluorides, has been prepared by the reaction of TlF with MoO_3 at 655°C. DSC shows two major polymorphic phase transitions at 42°C and 130°C, respectively. Electron diffraction and XRD studies of the complex room temperature polymorphic form of this material indicate that the spacegroup symmetry is monoclinic $P1a1$ with a superstructure unit cell given by $\mathbf{a} = 3\mathbf{a}_p + \mathbf{c}_p$, $\mathbf{b} = 3\mathbf{b}_p$, $\mathbf{c} = \frac{1}{2}(-\mathbf{a}_p + 3\mathbf{c}_p)$, when expressed with respect to the underlying ideal elpasolite-type parent structure. This superstructure, while related, is not isomorphous to that recently reported for $K_3MoO_3F_3$. The existence of a shared subset of strong $\mathbf{G}_p \pm J/5[204]_p^*$ type satellite reflections suggests the existence of a common intermediate superstructure. A highly structured, three-dimensional continuous diffuse intensity distribution is observed in $Tl_3MoO_3F_3$ and $Rb_2KMoO_3F_3$. This suggests that a particular pattern of local O/F ordering and associated Mo ion shifts, recently shown to be responsible for the existence of this diffuse distribution in the case of $K_3MoO_3F_3$, may be common to the entire family of elpasolite-related $A_2BM^{VI}O_3F_3$ compounds.

© 2003 Elsevier Science (USA). All rights reserved.

1. Introduction

There exists a relatively large number of oxyfluoride phases ($A_2^+ B^+ M^{VI}O_3F_3$; A, B = alkali metal; M^{VI} = Mo, W), which crystallize either in the ideal cubic ($Fm\bar{3}m$) A_2BMX_6 elpasolite structure type (see Fig. 1) or in closely related displacive variants thereof [1–10]. To date, such elpasolite-related oxyfluoride phases have been found for alkali elements ranging in size all the way from Na^+ to Cs^+. The ideal cubic A_2BMX_6 elpasolite, or parent, structure type (see Fig. 1) usually occurs in such materials only as a high temperature polymorphic form (the γ-polymorph). On cooling, this high temperature γ-polymorph typically undergoes two reversible structural phase transitions (at temperature T_2 to a β-polymorph and at temperature T_1 to a lowest temperature α-polymorph) [2–10]. Both these lower temperature polymorphic forms have been reported to be simulta-

neously ferroelectric as well as ferroelastic. As a result, the optical and dielectric properties of the materials have been extensively investigated [2–10]. Their rather complex crystallography, however, is far less well understood [2–7,11,12].

When the alkali elements are K, Rb or Cs (A, B = K, Rb, Cs), the first phase transition at temperature T_2 has been attributed to a spontaneous ferroelastic distortion of the metric symmetry of the parent structure from cubic to tetragonal [1–4]. The subsequent second phase transition to the α-polymorph, on cooling below T_1, has been reported to be correlated with the appearance of additional satellite reflections, i.e., to the onset of a superstructure [2–4,11,12]. The unit cell and symmetry of this superstructure (typically the room temperature polymorph) has in the past been the subject of considerable speculation as it has been variously described as tetragonal, monoclinic, trigonal as well as triclinic, based on studies of $Rb_2KMoO_3F_3$ and $K_3MoO_3F_3$ [2–7]. A very recent electron diffraction study of the complex α-polymorph of $K_3MoO_3F_3$ [11] has resolved many of these inconsistencies and determined the symmetry, of at least this polymorph, to be

*Corresponding author. Electron Microscope Unit, Research School of Biological Sciences, Australian National University, Canberra ACT 0200, Australia. Fax: +61-2-6125-3218.

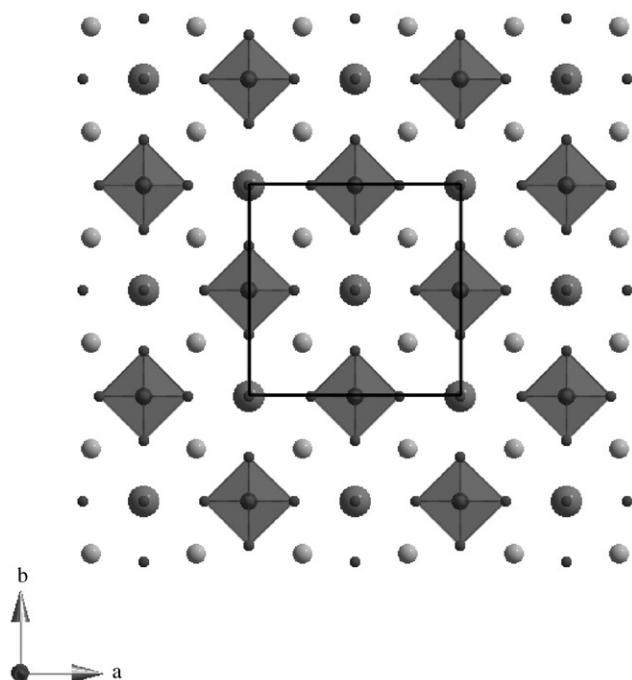*E-mail address:* brink@rsbs.anu.edu.au (F.J. Brink).

Fig. 1. Schematic (001) section of the ideal cubic ($Fm\bar{3}m$) A_2BMX_6 elpasolite type parent structure of $Tl_3MoO_3F_3$. The MoX_6 ($M =$ Mo, $X =$ anion) octahedra are highlighted and the parent unit cell marked. The A-type Tl ion is represented by the large dark ball, the B-type Tl ion by the medium gray ball and the anions (X) by the small balls.

monoclinic $I1a1$ ($\mathbf{a} = 2\mathbf{a}_p - \mathbf{c}_p$, $\mathbf{b} = 4\mathbf{b}_p$, $\mathbf{c} = \mathbf{a}_p + 2\mathbf{c}_p$; $\mathbf{a}^* = \frac{1}{10}[40\bar{2}]_p^*$, $\mathbf{b}^* = \frac{1}{8}[020]_p^*$ and $\mathbf{c}^* = \frac{1}{10}[204]_p^*$, when indexed with respect to the underlying parent structure, subscript p).

When the alkali element in the 12-coordinate A-site is Na^+, the crystallographic behavior changes subtly, but quite distinctly [8,9]. While there apparently still exist two structural phase transitions, the metric symmetry of the intermediate phase is no longer tetragonal, but reportedly monoclinic and pseudo-orthorhombic [8,9]. Clearly the relative size of the alkali and transition metal ions plays an important role in the structural behavior of these elpasolite-related oxyfluoride phases.

As part of an attempt to widen the compositional range of existence of this family of elpasolite-related oxyfluoride phases as well as to study the effect of relative ionic sizes upon their crystallography, we have investigated the possibility that thallium might be able to be used as a pseudo-alkaline substitute in these materials. While thallium has very similar chemistry to that of the alkaline group as far as chalcogenide compounds are concerned, it behaves quite differently to alkaline metals in some of its halogen chemistry. In the latter area, its chemistry has more similarities with that of the more polarizing Ag^+ ion [13]. Nonetheless, based purely on the similarity in ionic size of Tl^+ to that of K^+ and Rb^+, we might expect $Tl_3MoO_3F_3$ to crystallize in the elpasolite structure type or in a closely related variant thereof.

2. Experimental

2.1. Synthesis

The elpasolite-related $Tl_3MoO_3F_3$ successfully synthesized in this study was initially prepared in a similar manner to that previously reported for the alkaline analogue compounds [2–12], i.e., by the reaction of a 1:3 molar ratio of MoO_3 (Halewood Chemicals Ltd., 99.999%) with the appropriate anhydrous AF alkaline fluoride, in this case anhydrous TlF (Aldrich 99%), in a sealed platinum capsule heated at 655°C for 4 days.

Subsequently, it was discovered that $Tl_3MoO_3F_3$ could also be successfully synthesized by mixing the starting reagents, pressing into a pellet and heating in a sealed, evacuated quartz tube at temperatures as low as 130°C for 7 days. The very low temperature required for synthesis was unexpected but quite reproducible. In each synthetic method it was found to be essential that all reactants were manipulated in a dry box under dry argon to minimize contamination with air or water vapor.

2.2. Characterization

XRD data was collected using a Guinier-Hägg camera and $CuK\alpha_1$ radiation. Si (NBS #640c, $a = 5.431195(9)$ Å at 22.5°C) was used as an internal standard in order to accurately determine unit cell parameters.

Thermal analysis was used to detect the presence and temperature of any phase transitions and was carried out using a Mettler TA 4000 differential scanning calorimeter (DSC), under a constant flow nitrogen atmosphere. The scan rate used was 10°K/min and the sample weight was 26.2 mg. The transition temperatures given are the mean of the onset temperatures for the cooling and heating cycles. No significant weight-loss of the sample was noted.

Samples suitable for transmission electron microscope (TEM) work were prepared by the dispersion of finely ground material onto a holey carbon film. Electron diffraction patterns (EDPs) were obtained with a Philips EM 430 TEM. The sample was held in a Gatan liquid nitrogen cold stage at a temperature of ~ 80 K in order to prevent melting/decomposition of the sample due to beam induced heating.

3. Results and discussion

3.1. XRD

A scanned trace of a typical Guinier XRD pattern of room temperature $Tl_3MoO_3F_3$ over the 2θ range from 16° to 54° is shown in Fig. 2. (This should be compared
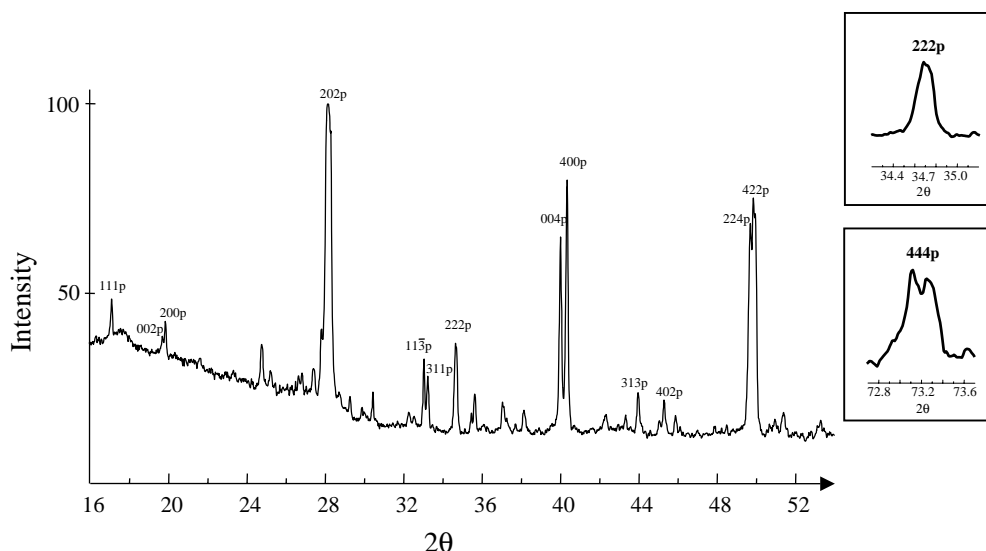
Fig. 2. A scanned trace of the room temperature Guinier XRD pattern of $Tl_3MoO_3F_3$ from $16°$ to $54°$ in 2θ. The strong parent reflections are labelled with a subscript p while the numerous, rather weak, additional satellite reflections are unlabelled. Note that the metric symmetry of the underlying parent sub-structure is very close to tetragonal. Splitting of the $\langle 444 \rangle_p^*$ line (inset) and broadening of the $\langle 222 \rangle_p^*$ line (inset), however, indicate that the metric symmetry is in fact monoclinic rather than tetragonal.

with the equivalent, clearly related Guinier trace for $K_3MoO_3F_3$ shown in Fig. 7 of [11]). The parent reflections are shown labelled with a subscript p. In addition to these strong parent reflections, note that there also exist numerous rather weak additional satellite reflections which could not all be unambiguously indexed even after the results of the electron diffraction study (see below).

As expected, the strongest reflections ($\langle 220 \rangle_p^*$, $\langle 004 \rangle_p^*$, $\langle 224 \rangle_p^*$, etc.) belong to the underlying F-centered parent sub-structure. Note that the $\langle 111 \rangle_p^*$ and $\langle 222 \rangle_p^*$ lines appear not to be split, whilst the $\langle 002 \rangle_p^*$ and $\langle 004 \rangle_p^*$ lines have clearly separated into two distinct lines with an intensity ration of 1:2. This indicates that, just as was the case for $K_3MoO_3F_3$, the metric symmetry of the room temperature polymorph of $Tl_3MoO_3F_3$ is again very close to tetragonal. Refinement of the underlying parent sub-structure cell dimensions on this assumption gave lattice parameters $\mathbf{a}_p = \mathbf{b}_p = 8.928(1)$ Å and $\mathbf{c}_p = 8.998(1)$ Å, approximately 3% bigger than the equivalent tetragonal parent cell dimensions of $K_3MoO_3F_3$ [11].

At high angle there was evidence of a slight monoclinic deviation in metric symmetry away from tetragonal in that the $\langle 444 \rangle_p^*$ line was narrowly but clearly split into two lines (see the inset). The $\langle 222 \rangle_p^*$ line, while not split, was broadened (see inset). Likewise, the $\langle 224 \rangle_p^*$ line was also narrowly split into three rather than two lines. Re-refinement of the underlying parent sub-structure cell dimensions, this time on the assumption of monoclinic metric symmetry, gave lattice parameters $\mathbf{a}_p = 8.928(1)$ Å, $\mathbf{b}_p = 8.998(1)$ Å, $\mathbf{c}_p = 8.928(1)$ Å and $\beta = 89.88(1)°$.
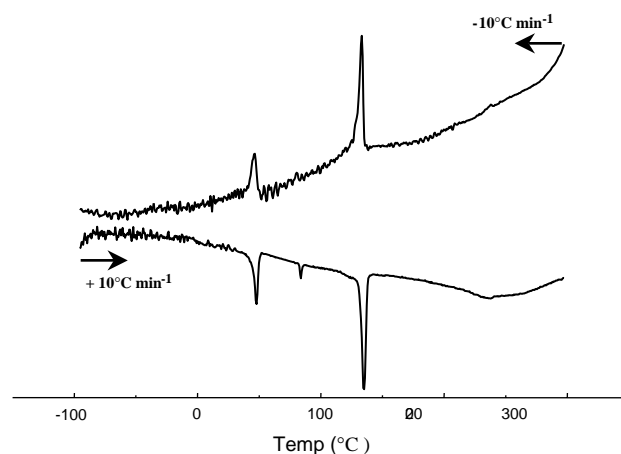

Fig. 3. DSC traces showing two strong, reproducible, phase transitions on both heating and cooling at $42(2)°C$ and $130(3)°C$, respectively.

3.2. DSC

Typical DSC patterns recorded on heating and cooling between $-100°C$ and $+300°C$ are shown in Fig. 3. Two major (and quite reproducible, on both heating and cooling cycles as well as upon repeated cycling) phase transitions at $42(2)°C$ and $130(3)°C$ can be seen in these patterns. This is consistent with the general behavior of the previously studied members of the $A_2BM^{VI}O_3F_3$ family ($A, B = $ K, Rb, Cs, $M = $ Mo, W), which have been reported to undergo two reversible structural phase transitions (see Table 1) on cooling from the high temperature ideal cubic polymorph [2–7]. A further weak peak at $82°C$ on heating could be yet

Table 1
Reported polymorphic phase transition temperatures for a range of $A_2BM^{IV}O_3F_3$ compounds

	T_1 (K)	T_2 (K)
$K_3MoO_3F_3$	436	522
$K_3WO_3F_3$	414	452
$Rb_3MoO_3F_3$	423	538
$Tl_3MoO_3F_3$	315	403
$Rb_3WO_3F_3$	410	483
$Cs_3MoO_3F_3$	343	525
$Cs_3WO_3F_3$	309	459
$Rb_2KMoO_3F_3$	182	328
$Rb_2KWO_3F_3$		291
$Cs_2KMoO_3F_3$		
$Cs_2KWO_3F_3$		
$Cs_2RbMoO_3F_3$		413
$Cs_2RbWO_3F_3$		348

another phase transformation although this peak was found to diminish on repeated cycling.

3.3. Electron diffraction

The EDPs were obtained from a $Tl_3MoO_3F_3$ specimen mounted in a liquid N_2 cold stage (to increase specimen stability under electron beam irradiation and minimize electron beam damage, a common problem in TEM studies of these oxyfluoride phases). It is important to note that no indication of a lower temperature phase transition than the 42(2)°C phase transition was observed in DSC even when cooled to −150°C. The polymorph investigated is thus equivalent to the lowest, or room, temperature polymorph of $Tl_3MoO_3F_3$.

Fig. 4a shows a typical (untwinned or single domain) $[010]_p$ type zone axis EDP of this polymorph. For comparison purposes, the equivalent $[010]_p$ type zone axis EDP of the lowest temperature α-polymorph of $K_3MoO_3F_3$ is shown in Fig. 4b [11]. To all intents and purposes, the EDPs appear isomorphous. Both exhibit relatively intense $G_p \pm J/5[204]_p^*$ (G_p an allowed parent Bragg reflection, J = integer) type satellite reflections. Clearly, as for for α-$K_3MoO_3F_3$ [11], the mirrors perpendicular to a_p and c_p as well as the tertiary $\langle 101 \rangle_p$ type mirrors present in the parent structure are broken in this polymorph. The only immediately noticeable difference between the two patterns is the rather lower intensity of the parent $h\,0\,l$, $h + 0 + l = 4n + 2$ (n = integer), reflections to the parent $h\,0\,l$, $h + 0 + l = 4n$ (n = integer), reflections in Fig. 4a when compared to the equivalent reflections in Fig. 4b. Careful measurement of the relative reciprocal space magnitudes (in Å^{-1}) of $2a_p^*$ and $2c_p^*$ in Fig. 4a could not detect any splitting suggesting that the unique $\langle 002 \rangle_p^*$ line (cf. Fig. 2) is the $[020]_p^*$ line. Such small splittings however are difficult to measure directly from EDPs.

There are, nevertheless, clear differences between the reciprocal lattices of α-$Tl_3MoO_3F_3$ and α-$K_3MoO_3F_3$ [11]. Careful re-investigation and contrast enhancement of Fig. 4a (see the enlarged box in Fig. 4a), for example, reveals the presence of very weak $G_p \pm J/10[602]_p^*$ and $G_p \pm J/10[\bar{2}06]_p^*$, J odd, satellite reflections in the case of $Tl_3MoO_3F_3$ which are not present in the case of $K_3MoO_3F_3$. The existence of these weak satellite reflections suggests that the reciprocal lattice unit cell vectors of the $Tl_3MoO_3F_3$ superlattice run along the $[602]_p^*$, $[020]_p^*$ and $[\bar{2}06]_p^*$ directions, respectively. This has been unambiguously confirmed by a range of other zone axis EDPs. Fig. 5, for example, shows a $[10\bar{3}]_p$ zone axis EDP of $Tl_3MoO_3F_3$ orthogonal to the $[010]_p$ zone axis EDP of Fig. 4a. Note the presence of a multitude of satellite reflections of the form $G_p + J/20[602]_p^* + K/6[020]_p^*$ (integer J, K). (These can be broken into two classes of satellite reflection: a rather more intense sub-set of $G_p \pm J/5[204]_p^*$ type (e.g., $\frac{1}{10}[602]_p^* + [010]_p^* \equiv [111]_p^* - \frac{1}{5}[204]_p^*$, etc.) and the rather less intense remainder). While the equivalent $[10\bar{3}]_p$ zone axis EDP of α-$K_3MoO_3F_3$ is not available, satellite reflections of the form $G_p + J/10[602]_p^* + 2K/8[020]_p^*$ (J, K integers) would be expected given its supercell and space group symmetry [11]. Note the sextupling along the parent $[020]_p^*$ reciprocal lattice direction in the case of $Tl_3MoO_3F_3$ (in distinction to the octupling observed in the case of α-$K_3MoO_3F_3$; cf. Fig. 5 with Fig. 4a of [11]) and the 20-fold, rather than 10-fold, superlattice along the $[602]_p^*$ reciprocal lattice direction. Clearly the lowest temperature polymorph of $Tl_3MoO_3F_3$ is not entirely isomorphous to α-$K_3MoO_3F_3$.

The need for at least two (of the three) primitive reciprocal lattice basis vectors of $Tl_3MoO_3F_3$ to take the form $\frac{1}{20}[602]_p^*$ and $\frac{1}{6}[020]_p^*$ respectively is apparent from Fig. 5 as well as from EDPs taken at other appropriate zone axis orientations (see, for example, the $[\bar{2}31]_p$ and $[13\bar{3}]_p$ zone axis EDPs of Fig. 6). That the remaining primitive reciprocal lattice basis vector must take the form $\frac{1}{10}[\bar{2}06]_p^*$ is clear from integer indexation of these latter EDPs but most directly from the close to $[010]_p$ zone axis EDP shown in Fig. 7. This latter EDP was obtained from the same area as Fig. 4a by tilting ∼2–3° away from the exact $[010]_p$ zone axis orientation to bring up the very weak superlattice FOLZ (first order Laue zone) ring at a height of $\frac{1}{3}b_p^*$ (see Fig. 5) above the zero OLZ (ZOLZ) reflections of Fig. 4a. The $\frac{1}{20}[602]_p^* \times \frac{1}{10}[\bar{2}06]_p^*$ mesh of satellite reflections in this superlattice FOLZ ring confirms unequivocally that the only primitive reciprocal lattice unit cell consistent with all of the observed electron diffraction evidence is given by $a^* = \frac{1}{20}[602]_p^*$, $b^* = \frac{1}{6}[020]_p^*$ and $c^* = \frac{1}{10}[\bar{2}06]_p^*$. Indexation without the subscript "p" in Figs. 4–7 is with respect to this proposed reciprocal lattice unit cell. The corresponding (necessarily P-centered) real space unit cell is given by $a = 3a_p + c_p$, $b = 3b_p$, $c = \frac{1}{2}(-a_p + 3c_p)$.

Fig. 4. (a) A typical $\langle 010 \rangle_p$ type zone axis EDP of the α-polymorph of $Tl_3MoO_3F_3$ along with (b) the equivalent zone axis EDP for the α-polymorph of $K_3MoO_3F_3$. Indexation with the subscript p is with respect to the underlying parent sub-structure while indexation without the subscript is with respect to the $\mathbf{a} = 3\mathbf{a}_p + \mathbf{c}_p$, $\mathbf{b} = 3\mathbf{b}_p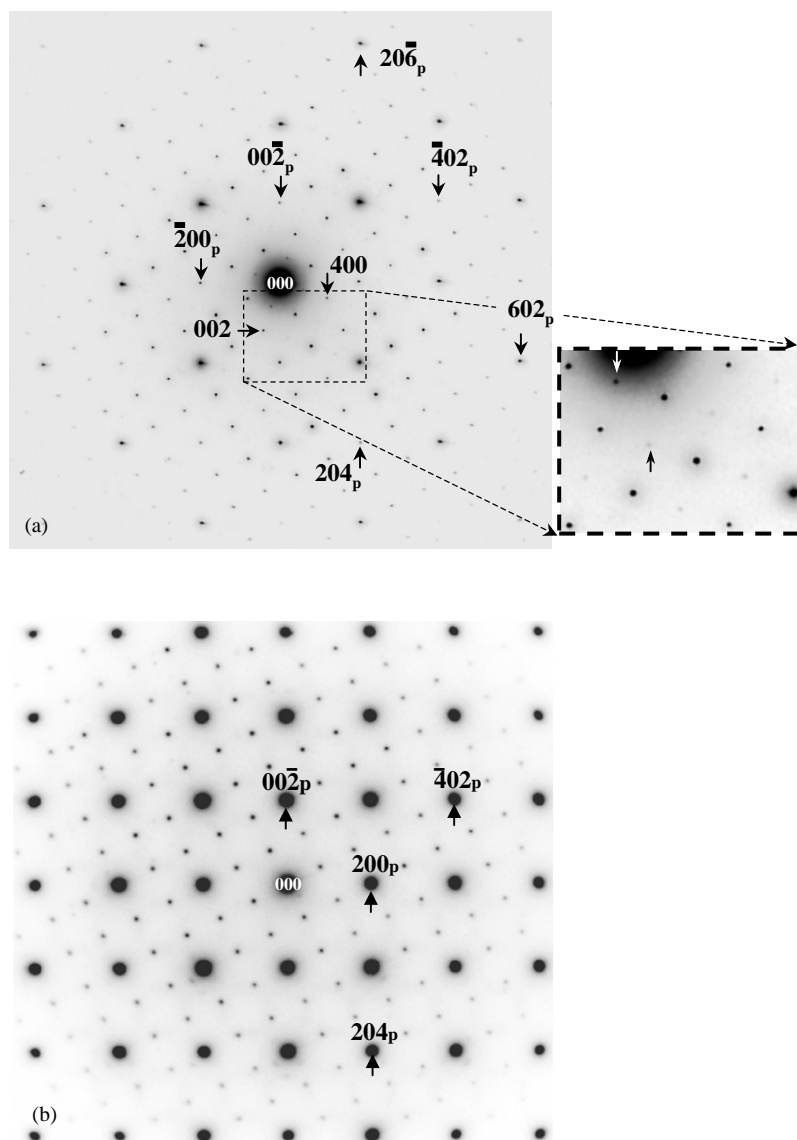$, $\mathbf{c} = \frac{1}{2}(-\mathbf{a}_p + 3\mathbf{c}_p)$ supercell. Note in each case the presence of the same $\mathbf{G}_p \pm J/5[204]_p^*$ ($J =$ integer) type superlattice reflections. Contrast enhancement of the region in the box in (a) reveals the presence of very weak $\mathbf{G}_p \pm J/10[602]_p^*$ and $\mathbf{G}_p \pm J/10[\bar{2}06]_p^*$, J odd, satellite reflections in the case of $Tl_3MoO_3F_3$ which are not present in the case of $K_3MoO_3F_3$.

Given the orientation of this supercell, the highest potential space group symmetry is thus monoclinic consistent with the monoclinic metric symmetry of the underlying parent sub-structure. The only potential zone axis orientation at which an extinction condition could conceivably occur (given the $Fm\bar{3}m$ parent structure space group symmetry) is thus $[010]_p$. The observed condition $F(h0l) = 0$ unless h is even in the ZOLZ at this zone axis orientation (see Fig. 4a) implies the presence of an a glide perpendicular to b. The resultant space group symmetry of α-$Tl_3MoO_3F_3$ is thus $P1a1$. (It has been assumed that the low temperature α-polymorph is ferroelectric thus ruling out the possibility of an inversion center).

Using the relationship between the resultant supercell and the parent unit cell ($\mathbf{a} = 3\mathbf{a}_p + \mathbf{c}_p$, $\mathbf{b} = 3\mathbf{b}_p$, $\mathbf{c} = \frac{1}{2}(-\mathbf{a}_p + 3\mathbf{c}_p)$) in conjunction with the above XRD refined parent unit cell dimensions gives $a = 28.251\,\text{Å}$, $b = 26.994\,\text{Å}$ and $c = 14.108\,\text{Å}$ with $\beta = 89.90°$. With such a large supercell and the very close to metrically tetragonal parent sub-cell, we were unable to unambiguously index all the weaker satellite reflections in the XRD data (particularly at higher 2θ). It is probable that the higher resolution attainable at a synchrotron will be essential to successfully and fully index all the observed satellite reflections let alone refine the corresponding crystal structure.
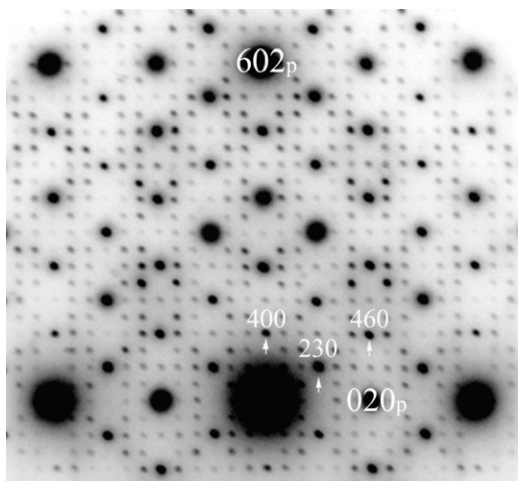
Fig. 5. A single domain $\langle 10\bar{3} \rangle_p$ ($\equiv$[100] supercell) zone axis EDP, orthogonal to the EDP shown in Fig. 4a. Indexation with the subscript p is with respect to the underlying parent sub-structure while indexation without the subscript is with respect to the $\mathbf{a} = 3\mathbf{a}_p + \mathbf{c}_p$, $\mathbf{b} = 3\mathbf{b}_p$, $\mathbf{c} = \frac{1}{2}(-\mathbf{a}_p + 3\mathbf{c}_p)$ supercell. Note the hierarchical intensity distribution of the superlattice reflections, with the $\mathbf{G}_p \pm J/5[204]_p^*$ class of satellite reflections significantly more intense than the remaining satellite reflections (note that $\frac{1}{10}[602]_p^* + [010]_p^* \equiv [111]_p^* - \frac{1}{5}[204]_p^*$, etc.).

3.3.1. Common intermediate superstructure?

While the resultant primitive unit cell for $Tl_3MoO_3F_3$, given by $\mathbf{a}^* = \frac{1}{20}[602]_p^*$, $\mathbf{b}^* = \frac{1}{6}[020]_p^*$ and $\mathbf{c}^* = \frac{1}{10}[\bar{2}06]_p^*$, is clearly non-isomorphous to that of $K_3MoO_3F_3$ ($\mathbf{a}^* = \frac{1}{10}[40\bar{2}]_p^*$, $\mathbf{b}^* = \frac{1}{8}[020]_p^*$ and $\mathbf{c}^* = \frac{1}{10}[204]_p^*$ [11]), there are nonetheless some striking similarities in their reciprocal lattices (cf. for example, Fig. 4a with b). The similarities are associated with a common and relatively intense sub-set of satellite reflections of the form $\mathbf{G}_p \pm J/5[204]_p^*$ ($J = 1$ or 2) while the differences are associated with rather weaker sets of additional satellite reflections (see Figs. 5 and 6). A similar effect was also observed in EDPs taken from $K_3MoO_3F_3$ (see, for example, Fig. 4 of [11]) which likewise shows $\mathbf{G}_p \pm J/5[204]_p^*$ type reflections to be of relatively higher intensity than the remaining $\mathbf{G}_p \pm J/10[204]_p^* \pm K/8[020]_p^*$ type reflections.

It therefore appears that the α-polymorphs of $Tl_3MoO_3F_3$ and $K_3MoO_3F_3$ share a common intermediate superstructure associated with these $\mathbf{G}_p \pm J/5[204]_p^*$ type satellite reflections of probable space group symmetry $I1m1$ ($\mathbf{a} = \frac{1}{2}(3\mathbf{a}_p + \mathbf{c}_p)$, $\mathbf{b} = \mathbf{b}_p$, $\mathbf{c} = \frac{1}{2}(-\mathbf{a}_p + 3\mathbf{c}_p)$; $\mathbf{a}^* = \frac{1}{10}[602]_p^*$, $\mathbf{b}^* = \frac{1}{2}[020]_p^*$, $\mathbf{c}^* = \frac{1}{10}[\bar{2}06]_p^*$). Such an intermediate superstructure appears to be common to the room temperature polymorphs of the entire family of $A_2BM^{VI}O_3F_3$ elpasolites since the same $\mathbf{G} \pm J/5[204]_p^*$ type satellite reflections have also been observed in EDPs taken from $Rb_2KMoO_3F_3$ (see Fig. 8) during a preliminary study on this very beam-sensitive compound. The resultant superstructures of the various $A_2BM^{VI}O_3F_3$ family members, as well as the close
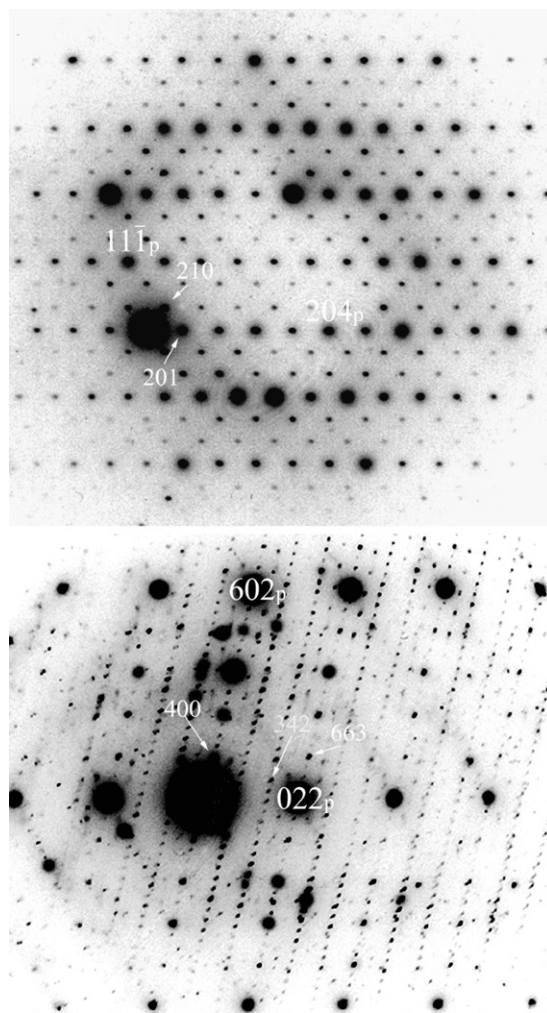

Fig. 6. An (a) $[\bar{2}31]_p$ ($\equiv[\bar{1}\,2\,2]$ supercell) zone axis EDP and (b) $[13\bar{3}]_p$ ($\equiv[01\bar{2}]$ supercell) zone axis EDP of the α-polymorph of $Tl_3MoO_3F_3$. Indexation with the subscript p is with respect to the underlying parent sub-structure while indexation without the subscript is with respect to the $\mathbf{a} = 3\mathbf{a}_p + \mathbf{c}_p$, $\mathbf{b} = 3\mathbf{b}_p$, $\mathbf{c} = \frac{1}{2}(-\mathbf{a}_p + 3\mathbf{c}_p)$ supercell.

structural relationships between them, therefore appear to be best described as distinct modulated variants of the same common underlying intermediate structure.

3.3.2. Characteristic diffuse intensity distribution

In addition to the sharp satellite reflections discussed above, the reciprocal lattice of $Tl_3MoO_3F_3$ simultaneously exhibits a highly structured, characteristic, diffuse intensity distribution very similar to that which occurs in the case of $K_3MoO_3F_3$ (see Fig. 9). So does the reciprocal lattice of $Rb_2KMoO_3F_3$ (see Fig. 10). The weakness of these distributions coupled with the sensitivity of the materials to electron beam irradiation, however, makes detailed investigation very difficult. In the case of $K_3MoO_3F_3$ [12], the observed diffuse distribution was shown to be well
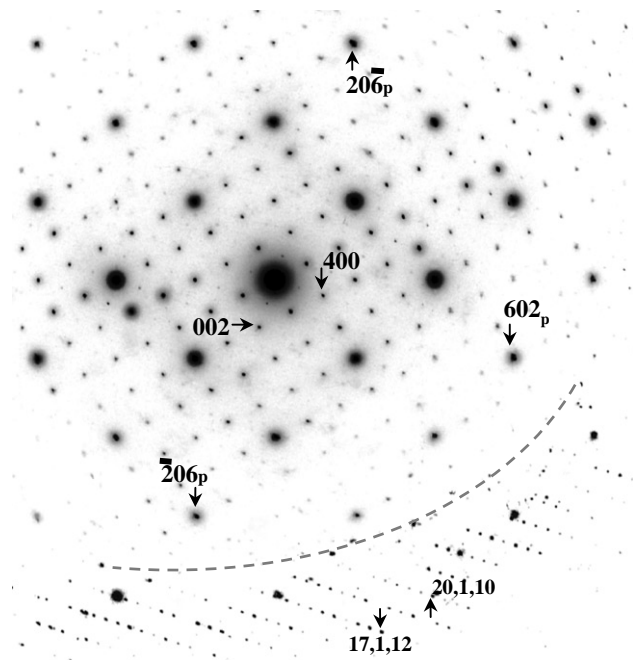
Fig. 7. Shows a close to $[010]_p$ zone axis EDP obtained from the same area as Fig. 4a by tilting ~ 2–3° away from the exact $[010]_p$ zone axis orientation to bring up the very weak superlattice FOLZ ring at a height of $\frac{1}{3}\mathbf{b}_p^*$ above the ZOLZ reflections of Fig. 4a. Note the $\frac{1}{20}[602]_p^*$ by $\frac{1}{10}[\bar{2}06]_p^*$ mesh of satellite reflections in the superlattice FOLZ ring. Indexation without the subscript p is with respect to the reciprocal lattice basis vectors $\mathbf{a}^* = \frac{1}{20}[602]_p^*$, $\mathbf{b}^* = \frac{1}{6}[020]_p^*$ and $\mathbf{c}^* = \frac{1}{10}[\bar{2}06]_p^*$.

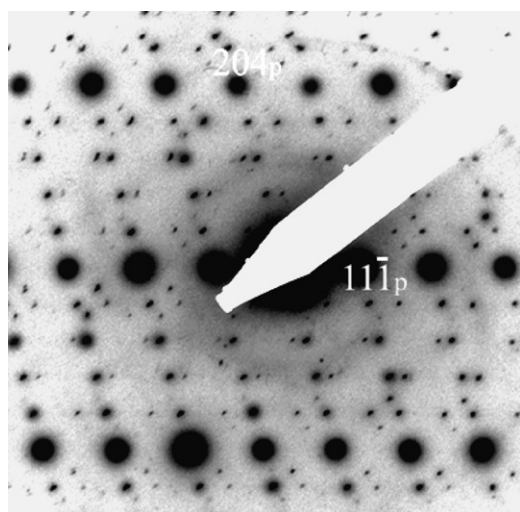Fig. 8. A $[\bar{1}32]_p$ zone axis EDP taken from $Rb_2KMoO_3F_3$. Indexation with the subscript p is with respect to the underlying parent sub-structure. Note the presence of the same $\mathbf{G} \pm J/5[204]^*$ type superlattice reflections.

described by the equation $\cos \pi h + \cos \pi k + \cos \pi l = 0$ when indexed with respect to the underlying parent sub-structure. Monte Carlo modelling was also used to show how local O/F ordering and associated induced Mo ion shifts could give rise to the observed characteristic diffuse intensity distribution [12]. The
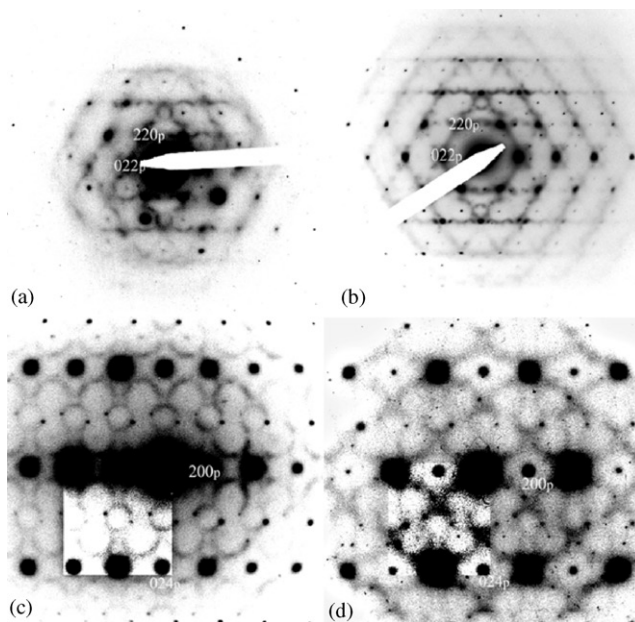

Fig. 9. Shows (a) $[11\bar{1}]_p$ and (c) $[02\bar{1}]_p$ zone axes EDPs of the lowest temperature α-polymorph of $K_3MoO_3F_3$ juxtaposed to the equivalent zone axis EDPs ((b) and (d)) for $Tl_3MoO_3F_3$. Note the strong similarity in the shape of the observed diffuse distribution.

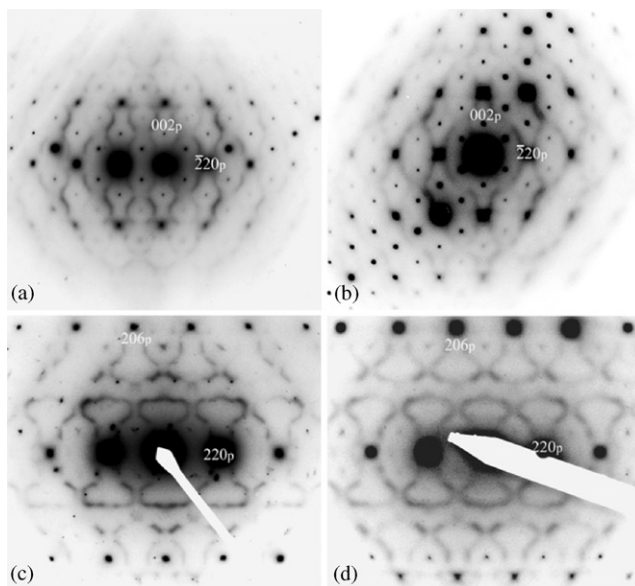Fig. 10. Shows (a) close to $[110]_p$ and (c) close to $[\bar{3}32]_p$ zone axes EDPs of the lowest temperature α-polymorph of $K_3MoO_3F_3$ juxtaposed to close to equivalent zone axis EDPs ((b) and (d)) for α-$Rb_2KMoO_3F_3$. Again note the strong similarity in the shape of the observed diffuse distribution.

similarity of the reciprocal space sections shown in Figs. 9 and 10 to the equivalent sections of $K_3MoO_3F_3$ suggests that such local O/F ordering (and associated Mo ion shifts) may well be common to the entire family of $A_2BM^{VI}O_3F_3$ oxyfluoride compounds.

4. Conclusions

The compositional range of existence of the $A_2BM^{VI}O_3F_3$ (A, B = alkali metal, M^{VI} = Mo, W) family of elpasolite-related oxyfluoride phases has been widened by the successful synthesis of elpasolite-related $Tl_3MoO_3F_3$. It has been shown that the complex superstructure characteristic of the low temperature α-polymorph of $Tl_3MoO_3F_3$ has monoclinic $P1a1$ space group symmetry and that, despite similarities, is not directly isomorphous to α-$K_3MoO_3F_3$. Nonetheless, the existence of a common subset of $\mathbf{G}_p \pm J/5[204]_p^*$ type satellite reflections in several different $A_2BM^{VI}O_3F_3$ room temperature polymorphs suggests the existence of a common intermediate superstructure which is then modulated in different ways to give rise to the various resultant superstructure polymorphs. Likewise, the observation of a very similar, highly structured diffuse intensity distribution in several different $A_2BM^{VI}O_3F_3$ room temperature polymorphs suggests that local O/F ordering (and associated Mo ion shifts) is common to the entire family of $A_2BM^{VI}O_3F_3$ oxyfluoride compounds.

References

[1] G. Pausewang, P. Rüdorff, Z. Anorg. Allg. Chemie 364 (1969) 69.
[2] G. Péradeau, J. Ravez, A. Tressaud, P. Hagenmuller, H. Arend, G. Chanussot, Solid State Commun. 23 (1977) 543.
[3] G. Péradeau, J. Ravez, H. Arend, Solid State Commun. 27 (1978) 515.
[4] G. Péradeau, J. Ravez, P. Hagenmuller, H. Arend, Solid State Commun. 27 (1978) 591.
[5] S.C. Abrahams, J.L. Bernstein, J. Ravez, Acta Crystallogr. B 37 (1981) 1332.
[6] J. Ravez, G. Péradeau, H. Arend, S.C. Abrahams, P. Hagenmuller, Ferroelectrics 26 (1980) 767.
[7] Z.G. Ye, J. Ravez, J.-P. Rivera, J.-P. Chaminade, H. Schmid, Ferroelectrics 124 (1991) 281.
[8] J.P. Chaminade, M. Cervera-Marzal, J. Ravez, P. Hagenmuller, Mater. Res. Bull. 21 (1986) 1209.
[9] J.P. Chaminade, M. Cervera-Marzal, J. Ravez, Mater. Sci. Eng. B 3 (1989) 497.
[10] M. Fouad, J.P. Chaminade, J. Ravez, A. Sadel, J. Solid State Chem. 124 (1996) 123.
[11] F.J. Brink, R.L. Withers, K. Friese, G. Madariaga, L. Norén, J. Solid State Chem. 163 (2002) 267.
[12] R.L. Withers, T.R. Welberry, F.J. Brink, L. Norén, J. Solid State Chem. 170 (2003) 211.
[13] N.N. Greenwood, A. Earnshaw, Chemistry of the Elements, 2nd Edition, Butterworth-Heinemann, Oxford, 1997, p. 226.